Published in final edited form as:
J Med Chem. 2013 December 12; 56(23): 9655–9663. doi:10.1021/jm401254c.

Characterization of a Novel Alpha-Conotoxin TxID from *Conus textile* that Potently Blocks rat Alpha3beta4 Nicotinic Acetylcholine Receptors

Sulan Luo[*,†], **Dongting Zhangsun**[†], **Xiaopeng Zhu**[†], **Yong Wu**[†], **Yuanyan Hu**[†], **Sean Christensen**[‡], **Peta J. Harvey**[§], **Muharrem Akcan**[§], **David J. Craik**[§], and **J. Michael McIntosh**[‡]

[†]Key Laboratory of Tropical Biological Resources, Ministry of Education, Key Lab for Marine Drug of Haikou, Hainan University, Haikou Hainan, 570228 China

[‡]Departments of Biology and Psychiatry, University of Utah, Salt Lake City, UT 84112 USA

[§]Institute for Molecular Bioscience, The University of Queensland, Brisbane, QLD 4072 Australia

Abstract

The α3β4 nAChRs are implicated in pain sensation in the PNS and addiction to nicotine in the CNS. We identified an α-4/6-conotoxin (CTx) TxID from *Conus textile*. The new toxin consists of 15 amino acid residues with two disulfide bonds. TxID was synthesized using solid phase methods and the synthetic peptide was functionally tested on nAChRs heterologously expressed in *Xenopus laevis* oocytes. TxID blocked rat α3β4 nAChRs with a 12.5 nM IC_{50}, which places it amongst the most potent α3β4 nAChR antagonists. TxID also blocked the closely related α6/α3β4 with a 94 nM IC_{50} but showed little activity on other nAChR subtypes. NMR analysis showed that two major structural isomers exist in solution, one of which adopts a regular α-CTx fold but with different surface charge distribution to other 4/6 family members. α-CTx TxID is a novel tool with which to probe the structure and function of α3β4 nAChRs.

Keywords

α-CTx; α3β 4 nAChRs; potent antagonist; NMR

INTRODUCTION

Nicotinic acetylcholine receptors (nAChRs) are ligand-gated cationic channels that mediate fast synaptic transmission[1] and are widely distributed throughout the peripheral and central nervous systems of both primitive and evolutionarily advanced organisms. In addition, presynaptic nAChRs induce various brain regions to release several neurotransmitters, including dopamine, norepinephrine, serotonin, and acetylcholine. nAChRs are implicated in the pathophysiology of a number of disease states including epilepsy, Alzheimer's disease, Parkinson's disease and addiction.

[*]Corresponding Author: Sulan Luo, Key Laboratory of Tropical Biological Resources, Ministry of Education, Hainan University; Haikou Hainan, 570228 China. Fax: (86) 898 66276720. luosulan2003@163.com.

The structures of nAChRs are highly conserved over a wide range of species from invertebrates to humans. This conservation is not only indicative of the important role that nAChRs play in the nervous system, but also provides an important platform for translational research from the *in vitro* discovery of selective ligands to their characterization *in vivo* in various animal models of human diseases.[2] In mammals there are 16 different nAChR subunits, α1–7, α9, α10 and β1-β4, as well as γ, δ , and ε. These subunits assemble into pentamers to form a complex variety of nAChR subtypes with distinct pharmacological and biophysical properties. nAChRs containing the α3 subunit are present in autonomic ganglia and modulate cardiovascular functions. Nociceptive cells in the dorsal root ganglia express α3 subunits and the correspondingα 3* nAChRs are likely to modulate pain sensation.

In the brain, the medial habenula expresses high nAChR levels.[3] The habenula is involved in anxiety, fear and the response to stress. Recently, α3* nAChRs present in the medial habenula have attracted substantial attention because of their potential role in influencing nicotine addiction. Blockage of cholinergic signaling in the medial habenula leads to signs of nicotine withdrawal.[4] Up- or down-regulation of nAChR function may influence the dose of nicotine that rodents will self-administer.[5–6] Thus, strategies to selectively modulateα 3* nAChR function are of considerable interest.

Conotoxins are peptides from the venom of the *Conus* genus of predatory marine snails; many of these toxins are potent antagonists of a range of ion channels, transporters and membrane receptors.[7–8] α-Conotoxins (α-CTxs) are amongst the smallest of the conopeptides (12–20 amino acid residues) and act as nAChR antagonists. The selectivity of α-CTxs isolated from different *Conus* species can vary markedly, thus enabling dissection of the functional roles of nAChR subtypes.

Defining the precise role of α3* nAChRs in normal and pathophysiological function has been hampered by the paucity of specific molecular probes. α-CTx AuIB from *Conus aulicus* has often been used, but its low potency has limited its use in physiological studies.[9] The current study characterized a novel α-CTx from *Conus textil*e. This peptide is the most potent α-CTx for α3β4 nAChRs yet reported, and represents a novel tool with which to probe the structure and function of α3β4 nAChRs.

RESULTS

DNA cloning and sequence analysis of the α-CTx TxID precursor

Each of the ~700 species of cone snail produces a unique, complex complement of venom peptides. The genes encoding these peptides may be grouped into superfamilies based on a highly conserved signal sequence. Within a superfamily, peptide families are defined by the arrangement of cysteines in the primary toxin sequence that is generally indicative of the peptide's ion channel target. In particular, the genes that encode α-CTxs show substantial conservation among all *Conus* species.[10–11] An intron that precedes the toxin sequence and the 3′ untranslated region are highly conserved. Primers were designed based on the conserved intron and 3′ untranslated region sequences and used to PCR-amplify the toxin-coding region of an α-CTx gene in *Conus textile*. A 170 base pair sequence was identified

that encodes a 16 amino acid toxin region (EMBL accession number HF543950). A glycine is present at the C-terminal cleavage site that predicts amidation of a 15 amino acid mature toxin with the sequence GCCSHPVCSAMSPIC* (* = C-terminal carboxamide). The mature peptide is also predicted to contain a cysteine pattern common to α-CTxs (CC-C-C). In contrast, the amino acid residues contained within the cysteine loops are unique, and are particularly divergent in the second cysteine loop compared to other known α-CTxs (Fig 1A and Table 1).

Chemical Synthesis and Oxidative Folding of α-CTx TxID

The predicted peptide was synthesized in a linear form using Fmoc chemistry (Fig. 1A, Table 2). The peptide had two sequential Cys residues near the N-terminus followed by two additional Cys residues. These four Cys residues may theoretically be connected in three different disulfide bond arrangements, although bridging of the vicinal Cys is less common in native peptides. Previously characterized α-CTxs purified from venom have a disulfide bond connectivity that links the first Cys to the third Cys and the second Cys to the fourth Cys.[12] We therefore synthesized α-CTx TxID with a bridging pattern of CysI-III and CysII-IV using directed two-step folding (Fig. 1B). We protected the cysteine side chains with two orthogonal protecting groups that can be removed selectively under different conditions, thus allowing the sequential formation of each disulfide bridge. S-trityl-protected cysteine was used for Cys2 and Cys8 and S-(acetamidomethyl) cysteine was used for Cys3 and Cys15. The acid labile S-trityl groups were removed first during cleavage from the resin while ferricyanide was used to close the disulfide bridge. The monocyclic peptide was purified by reverse-phase HPLC. Subsequently, the acid-stable acetomedomethyl groups were removed from the second and fourth Cys by iodine oxidation, which also closed the second disulfide bridge. The fully folded peptide was purified by HPLC with a retention time of 23.4 min (Fig. 1C). Laser desorption mass spectrometry (MALDI-TOF) of synthetic TxID was consistent with the presence of two disulfide bonds and an amidated C-terminus. TxID had calculated and observed monoisotopic masses of 1489.58 Da and 1489.5 Da, respectively. The synthetic peptide with the Cys2-Cys8 and Cys3-Cys15 disulfide bond arrangement was used in all subsequent studies(Fig. 1B).

Effect of α-CTx TxID on ACh-evoked currents through nAChRs

The functional effects of synthetic TxID were tested on a range of nAChR subtypes. Combinations of nAChR subunits were heterologously expressed in *Xenopus* oocytes and the response to ACh measured. Fig. 2 shows representative responses to ACh of α3β4, α3β2, α4β4 and α7 nAChRs in the presence and absence of TxID. A complete block of ACh-evoked currents was obtained with 1 μM TxID on α3β4 nAChR (Fig. 2A) compared with little or no blocking of α4β4 (Fig. 2B) α3β2 (Fig. 2C) and α7 (Fig. 2D) nAChRs by 10 μM TxID. The increased blockage of α3β4 nAChR activity by TxID was reversed within 4 minutes of toxin washout.

In contrast, when a β2 rather than a β4 nAChR subunit was co-expressed with the α3 subunit, the IC_{50} for TxID was more than 800-fold higher (Fig. 2B, Table 3), thus indicating that amino acid residue differences between the highly homologous β2 and β4 subunits significantly influence TxID toxin potency. Similarly, when an α4 rather than α3 nAChR

subunit was co-expressed with the β4 subunit, the IC_{50} for TxID was also > 1000-fold higher, again indicating that amino acid residue differences between the homologous α3 and α4 subunits significantly influence toxin potency (Fig.2 and Table 3).

α-CTx TxID showed a dose-dependent block of α3β4 receptors at low nanomolar concentrations with an IC_{50} of 12.5 (9.4–16.5) nM (Fig. 2E, Table 3). The concentration responses for TxID were subsequently assessed on each of the other expressed nAChR subtypes. α-CTx TxID was the next most potent on α6/α3β4 receptors with an IC_{50} of 94.1 (73–121) nM. TxID showed only weak blockage of α2β4 receptors with an IC_{50} of 4550 (3950–5230) nM. The IC_{50} for TxID was >10 μM for all other tested nAChR subtypes, including α3β2, α4β4, α4β2, α6/α3β2β3, α2β2, α9α10, α7, α1β1δε (Fig. 2B and Table 3). An ACh concentration-curve was performed on α3β4 nAChRs. Block of α3β4 nAChRs was then assessed in the presence of 10 μM TxID. With the addition of toxin to ACh, the magnitude of the maximum ACh response was reduced consistent with non-competitive block (Fig. 2F).

NMR Spectroscopy

To determine the three-dimensional solution structure of TxID, one-and two -dimensional NMR spectra were recorded at 280, 298 and 308 K. Spectra in 10% D_2O/90% H_2O showed more than the expected number of peaks which suggested *cis-trans* isomerisation of one or both of the two proline residues, as reported previously for other α-conotoxins.[13–16] A change of conditions to 30% d3-TFE/70% H_2O at 308 K resulted in spectra showing two major species in a ratio of approximately 40:60. Isomer 1 was assigned as the *trans-trans* isomer due to NOEs observed between the $H\alpha_{i-1}$–$H\delta_{Pi}$ protons of the Pro6 and Pro13 and their preceding residues. Cβ and Cγ chemical shifts were also used to assign both prolines as having *trans* peptide bond conformations.[17] Full assignment was not possible for this isomer as no amide protons were observed in the NOESY fingerprint region for Gly1, Cys2 and Val7, although the sidechain protons of Cys2 and Val7 could be observed in other regions of the spectrum, as well as sequentially from the NH protons of their following residues. In contrast, isomer 2 showed greater dispersion in the amide fingerprint region and showed a complete cycle of $H\alpha_i$–NH_{i+1} sequential connectivities, with the exception of the two proline residues (Pro6 and Pro13), which lack NH protons, and Gly1 at the N-terminus. Isomer 2 was determined to be a *cis-trans* isomer due to the lack of NOEs between $H\alpha_5$–$H\delta_6$ protons and alarge difference between the C βand C γchemical shifts of Pro6.

Structure Determination of TxID

Structure calculations were performed with CYANA using a torsion angle simulated annealing protocol. Distance and dihedral angle restraints were derived from the NOESY spectra and coupling constants, respectively. A set of structures consistent with the experimental data were calculated and the 20 lowest energy structures were chosen to represent the structural ensemble for each isomer (Fig. 3). A comparison of the structural statistics for each isomer is given in Table 4. Isomer 1 had a root mean square deviation (RMSD) of 0.48 ± 0.36 Å across backbone residues 2–15 and PROMOTIF [18] identified a short 3,10-helix spanning residues 8–10. In contrast, isomer 2 had an RMSD of 0.45 ± 0.25 Å and no secondary structural elements identified other than the two disulfide bonds.

DISCUSSION AND CONCLUSION

Cone snails hunt a variety of prey, including fish, mollusks and worms. They utilize nAChR antagonists as part of an arsenal of toxins to immobilize their prey. We identified a novel α-CTx encoded by a gene present in the mollusk-hunting *Conus textile* . The predicted mature toxin was synthesized and pharmacologically characterized. The peptide is most potent on α3β4 nAChRs (12.5 nM IC_{50}). α-CTx TxID is 7.5-fold less active on the closely related α6/α3β4 nAChR subtype and > 300-fold less active on all other tested nAChR subtypes (Table 2 and Table 3). α-CTx TxID is the most potent α-CTx antagonist of α3β4 nAChR yet characterized and has a unique selectivity profile.

The number of residues encompassed within the two loops (*m*, *n*) of α-CTxs is the basis for the division into several structural subgroups (*m/n*: 3/5, 4/3, 4/4, 4/5, 4/6 and 4/7). The loop-size roughly correlates with the pharmacological target selectivity. α-CTxs with a 3/5 framework are generally isolated from fish-hunting snails and are active towards fish and/or mammalian neuromuscular nAChRs, whereas CTxs from the 4/3, 4/4, 4/5, 4/6 or 4/7 classes mainly interact with mammalian neuronal nAChRs.[8] The most commonly reported framework is the 4/7 subgroup. Notably, the only other 4/6 peptide to be pharmacologically characterized is α-CTx AuIB, which was isolated from another mollusk-hunting cone snail, *Conus aulicus*.[9] AuIB also targets the α3β4 nAChR, but is 60-fold less active than the α-CTx TxID characterized here. AuIB also shows activity towards the α7 nAChR subtype, a feature not shared by TxID.[9,19–20] Other peptides isolated from worm- and fish-hunting *Conus* also show activity on α3β4 nAChRs, but lack the selectivity of α-CTx TxID. For example, an α4/7 -CTx RegIIA from *Conus regius* venom potently blocks α3β2, α3β4 and α7 nAChRs. RegIIA at 1 μM completely inhibited α3β2, α3β4 and α7 nAChRs and inhibited α9α10 receptors by 22%.[21] In contrast, whereas 1 μM TxID completely inhibited α3β4, 10 μM TxID produced no inhibition of α3β2, α4β4, α7 and α9α10 nAChRs. The α4/4-CTx BuIA from the fish-eating snail *Conus bullatus* potently blocks numerous rat nAChR subtypes, with the highest potency for α3- and chimeric α6-containing nAChRs.[22] The known related α-CTxs and their nAChR subtype selectivity preferences, including α3β4 nAChRs, are shown in Table 2.

α-CTx TxID has an SHP-sequence in its first loop, which is present in several other α-CTxs that differ in their specificity for nAChR subtypes (Tables 1, 2), indicating that the selectivity of TxID is probably determined by residues present in its second loop. The second loop of TxID contains -SAMSP-, a sequence that is not found in other pharmacologically tested α-CTxs and that may be important for the toxin's unique selectivity preference and potency towards the α3β4 nAChR subtype. The proline residue in the first loop of TxID is also noteworthy, as *cis-trans* isomerism at this residue might play a role in the overall conformation of TxID and related peptides, such as α4/6-AuIB, and α4/7-RegIIA, PeIA, PIA and Vc1.1 (Table 2). The NMR studies undertaken here showed that at least two structural isomers are present in TxID.

In the present study we synthesized TxID with disulfide connections between CysI-CysIII and CysII-CysIV (Fig. 1B) to match the disulfide configuration of native conotoxins isolated from venom. We note, however, an interesting report[20] that indicated that the ribbon (non-

native) isomer of the α4/6 conotoxin AuIB exhibited a 10-fold increase in activity. It would be of interest to determine the activity of α-CTx TxID with CysI-CysIV and CysII-CysIII connectivity (i.e. ribbon isomer).

α3β4 nAChRs are known historically for their roles in the autonomic nervous system. However, more recent studies suggest that they may have prominence in a number of CNS areas. α-CTxs have been used widely as pharmacological tools to characterize nAChRs. Studies with α-CTx AuIB suggested a role for α3β4 nAChRs in olfactory bulb neurogenesis[23] and the modulation of olfactory perceptual learning.[24] Nicotinic activation increases the frequency of spontaneous inhibitory postsynaptic currents in the basolateral amygdala by acting on α3β4-containing nicotinic receptors on GABAergic neurons and may play an important role in modulating synaptic transmission in the amygdala.[25] Several studies suggest that the α3β4 nAChRs are present in medial habenula neurons and affect nicotine self-administration.[26–27] In addition, the α3β4 combination may regulate glutamate release in hippocampal CA1 neurons.[28] Norepinephrine release from hippocampal synaptosomes is sensitive to α-CTx AuIB,[9] implying a nicotine-evoked norepinephrine release pathway that involves α3β4-containing nAChRs.[29] Intrathecal administration of α-CTx AuIB into neuropathic rats reduced mechanical allodynia for up to 6 h without significant side effects, suggesting that α3β4 nAChR subunit-selective CTxs could be promising tools for examining the role of nAChRs in neuropathic pain.[30]

NMR structural studies of TxID were complicated by the presence of two major conformational isomers, which increased the difficulty of solving the solution structure of this peptide in comparison to samples that contain a single isomer. Since these isomers cannot be separated and indeed, if they are separated would in any case equilibrate with each other, it is very difficult to identify which of the two isomers possesses the bioactive conformation, which is a limitation that we should explicitly point out here. Nonetheless, the use a 900 MHz spectrometer allowed us to successfully solve the structures of both isomers in solution. The structures of the two major conformational isomers indicated that one of them possesses the common α-helical motif that is found in a majority of other α-conotoxins characterized to date.

As illustrated in Fig.4, an alignment of the lowest energy structures of the two 4/6 conotoxins AuIB and TxID shows that the peptide backbone atoms overlay well, with an RMSD of 1.49 Å. Surface analysis reveals that, despite the sequence variation, the two peptides have a similar type of surface in terms of biophysical properties on one face and a different surface characteristic on the other face. Specifically, AuIB has a negatively charged Asp residue at position 14 whereas TxID has a hydrophobic Ile residue in the corresponding surface location. Given the similarities in fold, it would appear that this difference in surface properties is probably the reason for higher selectivity of TxID on α3β4 nAChRs. It will be of interest to test this hypothesis in future studies aimed at modulating the surface properties in this region.

In summary, we discovered and characterized a novel α4/6-CTx TxID that potently blocks α3β4 nAChRs with a unique selectivity profile, showing the most potent (low nanomolar)

blockage of α3β4 nAChRs so far. Thus, α-CTx TxID may be a valuable tool for elucidating the diverse roles of α3β4 nAChRs in a variety of normal and pathophysiological functions.

EXPERIMENTAL SECTION

Materials

Conus textile specimens were collected from the South China Sea off Hainan Province. Marine animal DNA Isolation Kit were purchased from Tiangen Biochemistry Ltd. (Beijing, China). The pGEM-T easy vector system were purchased from TaKaRa Ltd.(Dalian, China). A reverse-phase HPLC analytical Vydac C18 column (5μm, 4.6 mm × 250 mm) and preparative C18 Vydac column (10μm, 22mm×250mm) were obtained from Shenyue (Shanghai City, China). Reagents for peptide synthesis were from GL Biochem (Shanghai, China). All other chemicals used were of analytical grade. Clones of rat α2-α7 and β2-β4, as well as mouse muscle α1β1δε cDNAs were kindly provided by S. Heinemann (Salk Institute, La Jolla, CA). Clones of β2 and β3 subunits in the high expressing pGEMHE vector were kindly provided by C.W. Luetje (University of Miami, Miami, FL).

Identification and Sequencing of a genomic DNA clone encoding α-CTx TxID

Genomic DNA from the *C. textile*venom gland bulb was isolated using a marine animal DNA Isolation Kit (Tiangen Biochemistry Ltd. Beijing, China). The procedure followed the manufacturer's suggested protocol for marine invertebrates as described previously.[31] The resulting genomic DNA was used as a template for PCR using oligonucleotides tailed for cloning that corresponded to the 3′-end of the intron preceding the toxin region of α-CTx pre-propeptides and the 3′-UTR (untranslated region) sequence of the α pre-propeptides.[32] Final PCR amplification was performed with a cycling protocol composed of an initial denaturation at 94 °C for 7 min, 35 cycles at 94 °C for 30 s, 50 °C for 1 min, 72 °C for 2 min, and terminated with a final extension at 72 °C for 10 min. The purified PCR products were inserted into the pGEMT Easy vector via TA cloning (TaKaRa). Positive colonies transformed with conopeptide precursor DNA inserts were sequenced by Sangon Ltd.

Chemical synthesis of TxID

TxID was assembled on an amide resin by solid-phase methodology using an ABI 433A peptide synthesizer and FastMoc (N-(9-fluorenyl) methoxycarbonyl) chemistry with standard side-chain protection, except for cysteine residues. Cys residues were protected in pairs with either S-trityl on Cys1 and Cys3, or S-acetamidomethyl on Cys2 and Cys4 (Fig. 1B). The peptides were removed from the solid support by treatment with reagent K (trifluoroacetic acid water ethanedithiol phenol thioanisole; 90:5:2.5:7.5:5, v/v/v/v/v). The released peptide was precipitated and washed several times with cold ether. A two-step oxidation protocol was used to fold the peptides selectively as described previously.[33] The monocyclic and bicyclic peptides were purified by HPLC on a reversed-phase C18 Vydac column using a linear gradient of acetonitrile (ACN): 0–40 min 15–50% solvent B, 40–50 min 50–100% solvent B. Solvent B is 0.5% trifluoroacetic acid (TFA) in 90% acetonitrile with the remainder being water. Solvent A is 0.65% TFA in H_2O. Absorbance was monitored at 214 nm. The purity of the monocyclic and bicyclic peptides were determined by monitoring absorbance at 214 nm during HPLC (≥95% purity). Matrix-assisted laser

desorption ionization (MALDI) time-of-flight mass spectrometry was utilized to confirm the identity of the products.

Electrophysiology

Capped cRNA for the various subunits was made using the mMessage mMachine *in vitro* transcription kit (Ambion, Austin, TX) following plasmid linearization. cRNA of the α6/α3 chimera was combined with cRNA of high expressing β2 and β3 subunits or β4 (in the pGEMHE vector) to give 200–500 ng/μl of each subunit cRNA. cRNAs of the other various regular subunits were combined to give 200–500 ng/μl of each subunit cRNA. Fifty nl of this mixture was injected into *Xenopus* oocytes as described previously, and incubated at 17 °C. Oocytes were injected within one day of harvesting and recordings were made 2–4 days post-injection. Oocytes were voltage-clamped and exposed to ACh and peptide as described previously.[34] For screening of receptor subtypes and for toxin concentrations of 10 μM and lower, once a stable baseline was achieved either ND-96 alone or ND-96 containing varying α-CTxs concentrations was manually preapplied for 5 min prior to agonist addition. All recordings were done at room temperature (~22 °C).

ACh Concentration Response was determined by previously described methods.[35] Briefly, to acquire ACh concentration-response data, a chamber constructed from a disposable 200-μl polypropylene pipette tip with a length of 50 mm and an internal diameter of 0.5 mm at the upstream or intake end and 5 mm at the downstream or exhaust end. The chamber was perfused at a rate of ~2 ml/min. To introduce ACh into the chamber, the perfusion was halted for 10s and 20 μl of ACh was manually applied to the chamber via a small circular hole upstream from the oocyte. Upon resumption of perfusion (which was started immediately following the introduction of ACh into the chamber). This procedure was repeated with increasing concentrations ACh in the presence or absence of 10 μM toxin. with a time interval between applications of ACh of 50s. Responses were normalized to the response at 1 mM ACh which was defined as 100%.

Data Analysis

The average of 5 control responses just preceding a test response was used to normalize the test response to obtain "% response." Each data point of the dose-response curve represents the average ± S.E. of at least three oocytes. The dose-response data were fit to the equation: $\%\,\mathrm{response}=100/[1+([\mathrm{toxin}]/\mathrm{IC50})\hat{}\,\mathrm{n_H}]$, where n_H is the Hill coefficient, by non-linear regression analysis using GraphPad Prism (GraphPad Software, San Diego, CA).

NMR spectroscopy

NMR spectra for TxID were recorded in 500 μL of either 10% D_2O/90% H_2O or 30% TFE/70% H_2O (pH 3.5) on a Bruker Avance 600 MHz or a Bruker Avance-II 900 MHz NMR spectrometer. One-dimensional and two-dimensional NMR experiments, including TOCSY using a MLEV-17 spin lock sequence, NOESY, and DQF-COSY spectra were recorded at 280, 298 and 308 K. Chemical shifts were referenced to internal 2,2-dimethyl-2-silapentane-5-sulfonate (DSS) at 0 ppm. The TOCSY and NOESY spectra were run with mixing times of 80 and 200 ms, respectively. Two-dimensional spectra were generally collected over 4096 data points in the *f*2 dimension and 512 increments in the *f*1 dimension

over a spectral width of 12 ppm. Spectra were processed with Topspin (Bruker) and assigned using the program CCPNMR with the sequential assignment protocol.[36]

Structure calculations

Distance restraints were derived from the NOESY spectrum using peak volumes. Dihedral angle restraints were determined from $^{3}J_{\text{HN-H}\alpha}$ coupling constants obtained from a one-dimensional ^{1}HNMR spectrum. The phi angles were restrained to −100 ± 80° for $^{3}J_{\text{HN-H}\alpha}$~ 7 Hz and −120 ± 30° for $^{3}J_{\text{HN-H}\alpha}$ >8 Hz. Structures were generated using CYANA[37] and final structures were assessed using PROCHECK-NMR[38] and PROMOTIF[18] . The 20 structures with lowest energy and best quality were chosen to represent the solution structure of each isomer of TxID.

Acknowledgments

This work was supported, in whole or in part, by the Program for State High-Tech Research and Development Project (863) of the Ministry of Science and Technology of China Grant 2012AA021706, International Science & Technology Cooperation Program of China Grant 2011DFR31210, National Natural Science Foundation of China Grant 81160503 & 41366002, Changjiang Scholars and Innovative Research Team in University Grant PCSIRT, IRT1123. This work was also supported by National Institutes of Health Grants GM48677 and GM103801, and Australian Research Council Grant 1093115. DJC acknowledges the support of a National Health & Medical Research Council Professorial Fellowship (APP1026501). The authors also acknowledge financial support provided by the Queensland State Government to the Queensland NMR Network facilities at The University of Queensland. A preliminary account of some of this work was presented in the patent literature (Luo, S., Zhangsun, D., Hu, Y., Zhu, X., Wu, Y., and McIntosh, J. M. (2012) A-conotoxin TxID/Txd1, its drug combination and application. Chinese patent literature. CN (201210325531.9) –A).

We thank Layla Azam, Cheryl Dowell, Baldomero Olivera, and Doju Yoshikami for their advice and help.

ABBREVIATIONS USED

CTx	Conotoxin
nAChRs	nicotinic acetylcholine receptors
BSA	bovine serum albumin
TOCSY	total correlation spectroscopy
NOESY	nuclear Overhauser effect spectroscopy
DQF-COSY	double-quantum filtered-correlated spectroscopy

References

1. Gotti C, Clementi F. Neuronal nicotinic receptors: from structure to pathology. Prog Neurobiol. 2004; 74:363–396. [PubMed: 15649582]
2. Klee EW, Ebbert JO, Schneider H, Hurt RD, Ekker SC. Zebrafish for the study of the biological effects of nicotine. Nicotine Tob Res. 2011; 13:301–312. [PubMed: 21385906]
3. Marks MJ, Smith KW, Collins AC. Differential agonist inhibition identifies multiple epibatidine binding sites in mouse brain. J Pharmacol Exp Ther. 1998; 285:377–386. [PubMed: 9536034]
4. Salas R, Sturm R, Boulter J, De Biasi M. Nicotinic receptors in the habenulo-interpeduncular system are necessary for nicotine withdrawal in mice. J Neurosci. 2009; 29:3014–3018. [PubMed: 19279237]
5. Fowler CD, Lu Q, Johnson PM, Marks MJ, Kenny PJ. Habenular alpha5 nicotinic receptor subunit signalling controls nicotine intake. Nature. 2011; 471:597–601. [PubMed: 21278726]

6. Paolini M, De Biasi M. Mechanistic insights into nicotine withdrawal. Biochem Pharmacol. 2011; 82:996–1007. [PubMed: 21782803]
7. McIntosh JM, Santos AD, Olivera BM. Conus peptides targeted to specific nicotinic acetylcholine receptor subtypes. Annu Rev Biochem. 1999; 68:59–88. [PubMed: 10872444]
8. Terlau H, Olivera BM. Conus venoms: a rich source of novel ion channel-targeted peptides. Physiol Rev. 2004; 84:41–68. [PubMed: 14715910]
9. Luo S, Kulak JM, Cartier GE, Jacobsen RB, Yoshikami D, Olivera BM, McIntosh JM. alpha-conotoxin AuIB selectively blocks alpha3 beta4 nicotinic acetylcholine receptors and nicotine-evoked norepinephrine release. J Neurosci. 1998; 18:8571–8579. [PubMed: 9786965]
10. Santos AD, McIntosh JM, Hillyard DR, Cruz LJ, Olivera BM. The A-superfamily of conotoxins: structural and functional divergence. J Biol Chem. 2004; 279:17596–17606. [PubMed: 14701840]
11. Corpuz GP, Jacobsen RB, Jimenez EC, Watkins M, Walker C, Colledge C, Garrett JE, McDougal O, Li W, Gray WR, Hillyard DR, Rivier J, McIntosh JM, Cruz LJ, Olivera BM. Definition of the M-conotoxin superfamily: characterization of novel peptides from molluscivorous Conus venoms. Biochemistry. 2005; 44:8176–8186. [PubMed: 15924437]
12. Nicke A, Wonnacott S, Lewis RJ. Alpha-conotoxins as tools for the elucidation of structure and function of neuronal nicotinic acetylcholine receptor subtypes. Eur J Biochem. 2004; 271:2305–2319. [PubMed: 15182346]
13. Han KH, Hwang KJ, Kim SM, Kim SK, Gray WR, Olivera BM, Rivier J, Shon KJ. NMR structure determination of a novel conotoxin, [Pro 7,13] alpha A-conotoxin PIVA. Biochemistry. 1997; 36:1669–1677. [PubMed: 9048550]
14. Park KH, Suk JE, Jacobsen R, Gray WR, McIntosh JM, Han KH. Solution conformation of alpha-conotoxin EI, a neuromuscular toxin specific for the alpha 1/delta subunit interface of torpedo nicotinic acetylcholine receptor. J Biol Chem. 2001; 276:49028–49033. [PubMed: 11641403]
15. Chi SW, Kim DH, Olivera BM, McIntosh JM, Han KH. Solution conformation of alpha-conotoxin GIC, a novel potent antagonist of alpha3beta2 nicotinic acetylcholine receptors. Biochem J. 2004; 380:347–352. [PubMed: 14992691]
16. Cho JH, Mok KH, Olivera BM, McIntosh JM, Park KH, Han KH. Nuclear magnetic resonance solution conformation of alpha-conotoxin AuIB, an alpha(3)beta(4) subtype-selective neuronal nicotinic acetylcholine receptor antagonist. J Biol Chem. 2000; 275:8680–8685. [PubMed: 10722709]
17. Hill JM, Alewood PF, Craik DJ. Three-dimensional solution structure of mu-conotoxin GIIIB, a specific blocker of skeletal muscle sodium channels. Biochemistry. 1996; 35:8824–8835. [PubMed: 8688418]
18. Hutchinson EG, Thornton JM. PROMOTIF--a program to identify and analyze structural motifs in proteins. Protein Sci. 1996; 5:212–220. [PubMed: 8745398]
19. Muttenthaler M, Akondi KB, Alewood PF. Structure-activity studies on alpha-conotoxins. Curr Pharm Des. 2011; 17:4226–4241. [PubMed: 22204424]
20. Dutton JL, Bansal PS, Hogg RC, Adams DJ, Alewood PF, Craik DJ. A new level of conotoxin diversity, a non-native disulfide bond connectivity in alpha-conotoxin AuIB reduces structural definition but increases biological activity. J Biol Chem. 2002; 277:48849–48857. [PubMed: 12376538]
21. Franco A, Kompella SN, Akondi KB, Melaun C, Daly NL, Luetje CW, Alewood PF, Craik DJ, Adams DJ, Mari F. RegIIA: an alpha4/7-conotoxin from the venom of Conus regius that potently blocks alpha3beta4 nAChRs. Biochem Pharmacol. 2012; 83:419–426. [PubMed: 22108175]
22. Azam L, Dowell C, Watkins M, Stitzel JA, Olivera BM, McIntosh JM. Alpha-conotoxin BuIA, a novel peptide from Conus bullatus, distinguishes among neuronal nicotinic acetylcholine receptors. J Biol Chem. 2005; 280:80–87. [PubMed: 15520009]
23. Sharma G. The dominant functional nicotinic receptor in progenitor cells in the rostral migratory stream is the alpha3beta4 subtype. J Neurophysiol. 2013; 109:867–872. [PubMed: 23136348]
24. D'Souza RD, Vijayaraghavan S. Nicotinic receptor-mediated filtering of mitral cell responses to olfactory nerve inputs involves the alpha3beta4 subtype. J Neurosci. 2012; 32:3261–3266. [PubMed: 22378897]

25. Zhu PJ, Stewart RR, McIntosh JM, Weight FF. Activation of nicotinic acetylcholine receptors increases the frequency of spontaneous GABAergic IPSCs in rat basolateral amygdala neurons. J Neurophysiol. 2005; 94:3081–3091. [PubMed: 16033935]
26. Grady SR, Moretti M, Zoli M, Marks MJ, Zanardi A, Pucci L, Clementi F, Gotti C. Rodent habenulo-interpeduncular pathway expresses a large variety of uncommon nAChR subtypes, but only the alpha3beta4* and alpha3beta3beta4* subtypes mediate acetylcholine release. J Neurosci. 2009; 29:2272–2282. [PubMed: 19228980]
27. McCallum SE, Cowe MA, Lewis SW, Glick SD. alpha3beta4 nicotinic acetylcholine receptors in the medial habenula modulate the mesolimbic dopaminergic response to acute nicotine in vivo. Neuropharmacology. 2012; 63:434–440. [PubMed: 22561751]
28. Alkondon M, Albuquerque EX. A non-alpha7 nicotinic acetylcholine receptor modulates excitatory input to hippocampal CA1 interneurons. J Neurophysiol. 2002; 87:1651–1654. [PubMed: 11877536]
29. Kulak JM, McIntosh JM, Yoshikami D, Olivera BM. Nicotine-evoked transmitter release from synaptosomes: functional association of specific presynaptic acetylcholine receptors and voltage-gated calcium channels. J Neurochem. 2001; 77:1581–1589. [PubMed: 11413241]
30. Napier IA, Klimis H, Rycroft BK, Jin AH, Alewood PF, Motin L, Adams DJ, Christie MJ. Intrathecal alpha-conotoxins Vc1. 1, AuIB and MII acting on distinct nicotinic receptor subtypes reverse signs of neuropathic pain. Neuropharmacology. 2012; 62:2202–2207. [PubMed: 22306793]
31. Zheng X, Gao B, Li B, Peng C, Wu Y, Zhu X, Chen X, Zhangsun D, Luo S. Primer screening for new alpha-conotoxin gene cloning. Biotechnology. 2012; 21:40–44.
32. McIntosh JM, Dowell C, Watkins M, Garrett JE, Yoshikami D, Olivera BM. Alpha-conotoxin GIC from Conus geographus, a novel peptide antagonist of nicotinic acetylcholine receptors. J Biol Chem. 2002; 277:33610–33615. [PubMed: 12114524]
33. Dowell C, Olivera BM, Garrett JE, Staheli ST, Watkins M, Kuryatov A, Yoshikami D, Lindstrom JM, McIntosh JM. Alpha-conotoxin PIA is selective for alpha6 subunit-containing nicotinic acetylcholine receptors. J Neurosci. 2003; 23:8445–8452. [PubMed: 13679412]
34. Cartier GE, Yoshikami D, Gray WR, Luo S, Olivera BM, McIntosh JM. A new alpha-conotoxin which targets alpha3beta2 nicotinic acetylcholine receptors. J Biol Chem. 1996; 271:7522–7528. [PubMed: 8631783]
35. Azam L, Yoshikami D, McIntosh JM. Amino acid residues that confer high selectivity of the alpha6 nicotinic acetylcholine receptor subunit to alpha-conotoxin MII[S4A,E11A,L15A]. J Biol Chem. 2008; 283:11625–11632. [PubMed: 18299323]
36. Wüthrich, K. NMR of Proteins and Nucleic Acids. Wiley-Interscience; New York: 1986. p. 130-135.
37. Guntert P, Mumenthaler C, Wuthrich K. Torsion angle dynamics for NMR structure calculation with the new program DYANA. J Mol Biol. 1997; 273:283–298. [PubMed: 9367762]
38. Laskowski RA, Rullmannn JA, MacArthur MW, Kaptein R, Thornton JM. AQUA and PROCHECK-NMR: programs for checking the quality of protein structures solved by NMR. J Biomol NMR. 1996; 8:477–486. [PubMed: 9008363]
39. Koradi R, Billeter M, Wuthrich K. MOLMOL: a program for display and analysis of macromolecular structures. J Mol Graph. 1996; 14:51–5. 29–32. [PubMed: 8744573]
40. Ellison M, Haberlandt C, Gomez-Casati ME, Watkins M, Elgoyhen AB, McIntosh JM, Olivera BM. Alpha-RgIA: a novel conotoxin that specifically and potently blocks the alpha9alpha10 nAChR. Biochemistry. 2006; 45:1511–1517. [PubMed: 16445293]
41. McIntosh JM, Plazas PV, Watkins M, Gomez-Casati ME, Olivera BM, Elgoyhen AB. A novel alpha-conotoxin, PeIA, cloned from Conus pergrandis, discriminates between rat alpha9alpha10 and alpha7 nicotinic cholinergic receptors. J Biol Chem. 2005; 280:30107–30112. [PubMed: 15983035]
42. Luo S, Akondi KB, Zhangsun D, Wu Y, Zhu X, Hu Y, Christensen S, Dowell C, Daly NL, Craik DJ, Wang CI, Lewis RJ, Alewood PF, McIntosh JM. Atypical alpha-conotoxin LtIA from Conus litteratus targets a novel microsite of the alpha3beta2nicotinic receptor. J Biol Chem. 2010; 285:12355–12366. [PubMed: 20145249]

43. Jakubowski JA, Keays DA, Kelley WP, Sandall DW, Bingham JP, Livett BG, Gayler KR, Sweedler JV. Determining sequences and post-translational modifications of novel conotoxins in Conus victoriae using cDNA sequencing and mass spectrometry. J Mass Spectrom. 2004; 39:548–557. [PubMed: 15170751]
44. Hu H, Bandyopadhyay PK, Olivera BM, Yandell M. Characterization of the Conus bullatus genome and its venom-duct transcriptome. BMC Genomics. 2011; 12:60. [PubMed: 21266071]
45. Kauferstein S, Porth C, Kendel Y, Wunder C, Nicke A, Kordis D, Favreau P, Koua D, Stocklin R, Mebs D. Venomic study on cone snails (Conus spp) from South Africa. Toxicon. 2011; 57:28–34. [PubMed: 20933537]
46. Ellison M, Gao F, Wang HL, Sine SM, McIntosh JM, Olivera BM. Alpha-conotoxins ImI and ImII target distinct regions of the human alpha7 nicotinic acetylcholine receptor and distinguish human nicotinic receptor subtypes. Biochemistry. 2004; 43:16019–16026. [PubMed: 15609996]
47. Vincler M, Wittenauer S, Parker R, Ellison M, Olivera BM, McIntosh JM. Molecular mechanism for analgesia involving specific antagonism of alpha9alpha10 nicotinic acetylcholine receptors. Proc Natl Acad Sci U S A. 2006; 103:17880–17884. [PubMed: 17101979]
48. Luo S, Zhangsun D, Wu Y, Zhu X, Hu Y, McIntyre M, Christensen S, Akcan M, Craik DJ, McIntosh JM. Characterization of a novel alpha-conotoxin from conus textile that selectively targets alpha6/alpha3beta2beta3 nicotinic acetylcholine receptors. J Biol Chem. 2013; 288:894–902. [PubMed: 23184959]

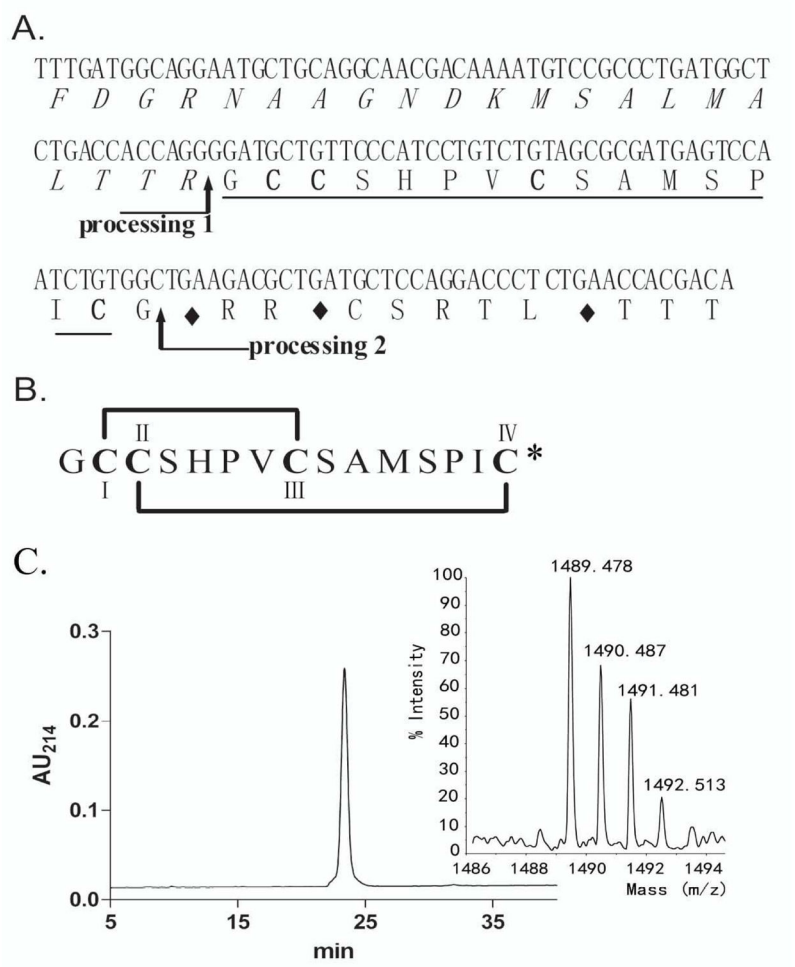

Figure 1.

α-CTx TxID pre-propeptide and encoded toxin (A), mature peptide sequence with a disulfide connectivity I–III, II–IV (B), and corresponding HPLC chromatograms (C) are shown (EMBL accession number HF543950). (A) A putative proteolytic processing site 1 (R) and amidation processing site 2 (G) are indicated by the arrow and the pro-region is in italics. The mature toxin region is underlined. The first glycine following the C-terminal cysteine in the mature toxin is presumed to be processed to a C-terminal amide in TxID. Cysteines are indicated in bold print. The stop codon is indicated by ◆. The deduced mature toxin sequence of TxID is GCCSHPVCSAMSPIC* (*, C-terminal carboxamide). (B) *, C-terminal carboxamide. (C) HPLC chromatograms of α-CTx TxID with a retention time of 23.4 min. The peptide was analyzed on a reversed phase analytical Vydac C18 HPLC using a linear gradient of 15% buffer B to 50% buffer B over 40 min, where A = 0.65% trifluoroacetic acid (TFA) and B = 0.5% TFA, 90% acetonitrile, and the remainder water. Absorbance was monitored at 214 nm. Inset in Figure 1C is MALDI-MS data for α-CTx TxID with observed monoisotopic mass of 1489.5 Da.

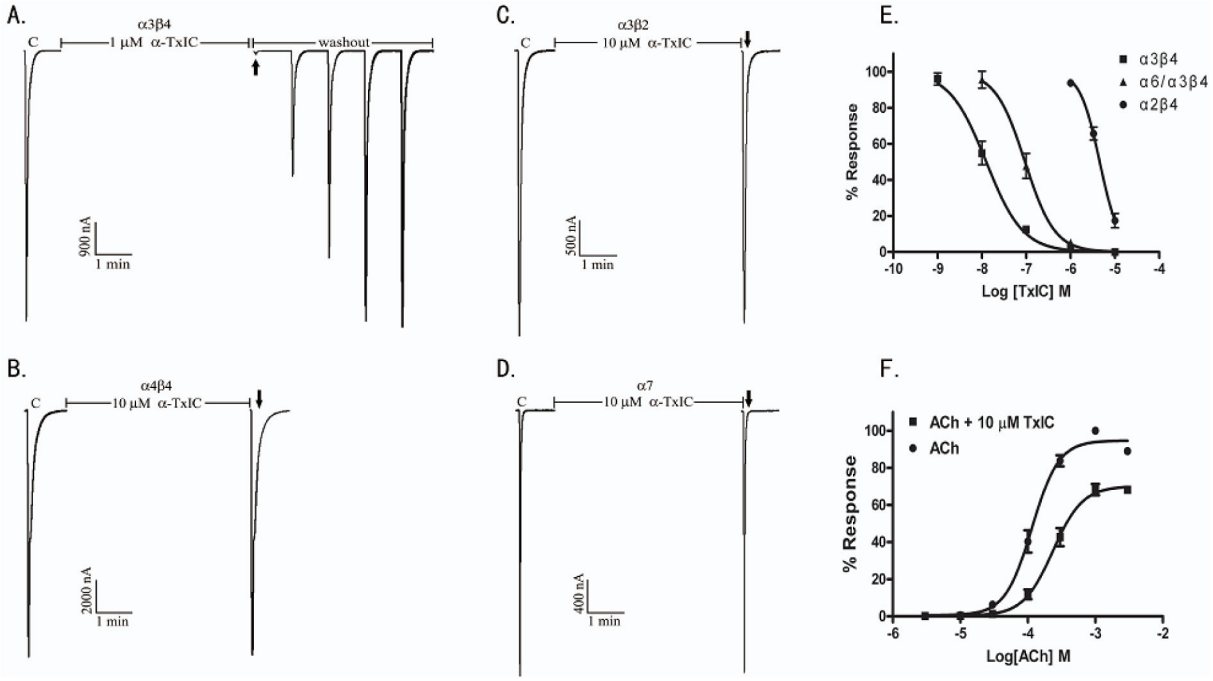

Figure 2.

The α-CTx TxID potently and selectively blocks α3β4 nAChRs. α-CTx TxID blocks α3β4 nAChRs (***A***) but has little or no activity at α4β4 (***B***), α3β2 (***C***) and α7 (***D***) subtypes. *Xenopus* oocytes expressing a given rat nAChR were voltage clamped at −70 mV and subjected to a 1 s pulse of ACh every minute as described in *Experimental Procedures* . A representative response in a single oocyte is shown. After control responses to ACh, the oocyte was exposed to 1 μM or 10 μM toxin for 5 min (arrow). The toxin was then washed out and the response to ACh was again measured. “C” indicates control responses to ACh. (*E*) Concentration response of α-CTx TxID on α3β4, α6/α3β4, α2β4 nAChR subtypes. Values are mean ± SEM from 3 to 8 separate oocytes. IC_{50} and Hill slope values are shown in Table 3. (*F*) ACh-concentration-response curve for α3β4 nAChRs in the absence and presence of 10μM α-CTx TxID. Data were obtained in duplicate for each concentration from 3 separate oocytes. Responses were normalized to 1 mM ACh (defined as 100%).

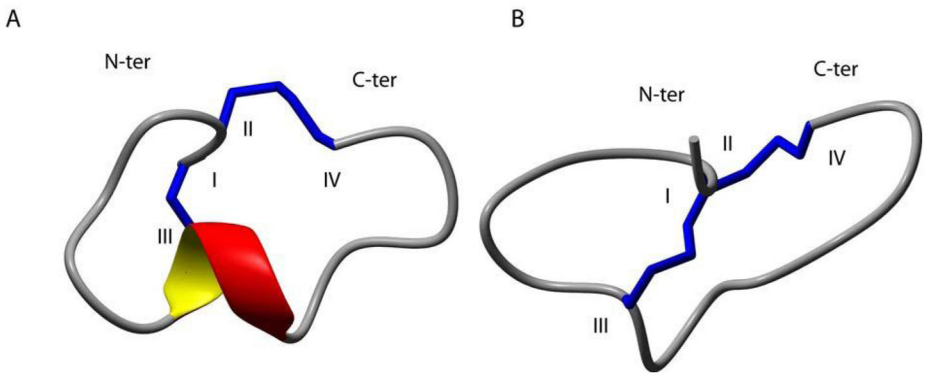

Figure 3.

Ribbon representation of the lowest energy structures of α-conotoxin TxID. *A*, Isomer 1. *B*, Isomer 2. The N- and C-termini are labeled with N-ter and C-ter, respectively. The α-helical region between residues Cys8 and Ala10 is shown in *red* and *yellow*. Cysteine residues are labeled with Roman numerals and disulfide bonds are shown in *blue*. The structures were generated using the program MOLMOL.[39]

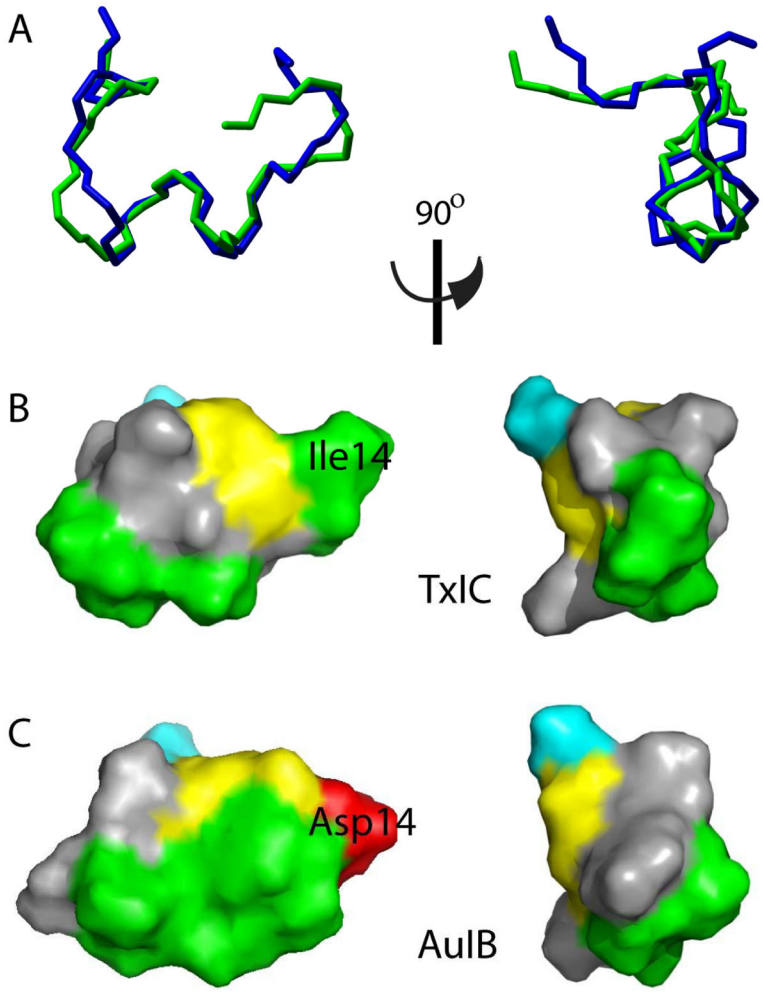

Figure 4.

Overlays and surface representations of TxID and AuIB. *A*, Overlays of TxID Isomer 1 (green) and AuIB (blue) (PDB code 1MXN). Lowest energy structures are aligned over the backbone atoms of residues from 2–15. Surface representation of *B*, TxID and *C*, AuIB. The negative residue (Asp) is shown in *red*, polar residues (Asn, His, Met, Ser, Thr and Tyr) are shown in *grey*, and hydrophobic residues (Ala, Ile, Phe, Pro, and Val) are *green*, cystines are *yellow*, and glycines are *cyan*. The images on the *right* are rotated the 90° around the horizontal axis. Surface representations were generated using the program PYMOL.

Table 1

Sequence alignment of TxID and related α-CTx precursors.

Precursor to		Species	Signal sequence	*Pro- region* ↓	mature region	Reference
α.m/n	**Peptide**					
α4/6	**TxID**	*C. textile*		*FDGRNAAGNDKMSALMALTTR*↓	GCCSHPVCSAMSP-ICG	This Study
	AuIB	*C. aulicus*	MFTVFLLVVLATTVVSFTS	*DRASDGRKDAASGLIALTMK*↓	GCCSYPPCFATNP-DCGRRR	9
α4/4	BuIA	*C. bullatus*	MFTVFLLVVLTTTVVSFPS	*DRASDGRNAAANDKASDVVTLVLK*↓	GCCSTPPCAVLY----CGRRR	22
α4/3	RgIA	*C. regius*		*SNKRKNAAMLDMIAQHAIR* ↓	GCCSDPRCRYR----CR	40
α4/7	PeIA	*C.pergrandis*		*FDGRNAAANDKASDLVALTVR*↓	GCCSHPACSVNHPELCG	41
	RegIIA	*C. regius*	MGMRMMGFTVFLLVVLTTTVVSSTS	*VRASDGRNAAADNRASDLIAQIVRR*↓	GCCSHPACNVNNPHICG	21
	LtIA	*C. litteratus*	MGMRMMFIMFMLVVLATTVVTFTS	*DRALDAMNAAASNKASRLIALAVR*↓	GCCARAACAGIHQELCGGGR	42
	MII	*C. magus*	MGMRMMFTVFLLVVLATTVVSFPS	*DRASDGRNAAANDKASDVITLALK*↓	GCCSNPVCHLEHSNLCGRRR	34
	Vc1.1	*C. victoriae*	MGMRMMFTVFLLVVLATTVVSSTS	*GRREFRGRNAAAKASDLVSLTDKKR*↓	GCCSDPRCNYDHPEICG	43

Signal sequence is shaded. The pro-region is in italics. A putative proteolytic processing site (R or K) is indicated by the arrow. The mature toxin region is underlined. *, C-terminal amidation, the first glycine following the C-terminal cysteine in the mature toxin is presumed to be processed to a C-terminal amide for the corresponding toxin. Cysteines are indicated in bold print and framed. Dashes denote gaps

J Med Chem. Author manuscript; available in PMC 2014 December 12.

Table 2

Sequence informationof related α-CTxs and their nAChR subtype selectivity preference and IC_{50}values.

αm/n[a]	**Peptide**	**Species**	**Sequence**[b]	**nAChRs selectivity (IC_{50}[nM][a])**	**Reference**
α4/6	**TxID**	*C. textile*	GCCSHPVCSAMSP-IC*	**α3β4 (12.5 nM)** > α6/α3β4 (94 nM) > α2β4 (4550 nM)	This Study
	AuIB	*C. aulicus*	GCCSYPPCFATNP-DC*	α3β4 (750 nM) > α7	9
	Bu22	*C. bullatus*	GCCTYPPCAVLSP-LCD	N.D.	44
	TiIA	*C. tinianus*	GGCCSHPAC-QNNPDyC*	N.D.	45
α4/4	BuIA	*C. bullatus*	GCCSTPPCAVLY---C*	α6/α3β2β3 (0.26 nM) >α6/α3β4 (1.54 nM) > α3β2 (5.72 nM)> α3β4 (27.7 nM > α4β4 (69.9 nM) > α2β4 (121 nM)> α7 (272 nM)>α2β2 (800nM)	22
α4/3	ImI	*C.imperialis*	GCCSDPRCAWR----C*	α3β2(41 nM) > α7(595 nM) >α9α10 (2000 nM) > α3β4 (3390 nM)	47
	RgIA	*C. regius*	GCCSDPRCRYR----CR	α9α10 (5.2 nM) > α7 (4700 nM)	40
α4/7	RegIIA	*C. regius*	GCCSHPACNVNNPHIC*	α3β2 (33 nM) > α3β4 (97 nM) > α7 (103 nM) > α9α10	21
	PeIA	*C.pergrandis*	GCCSHPACSVNHPELC*	α9α10 (6.9 nM) > α3β2 (23 nM) > α3β4 (480nM) > α7 (1800 nM)	41
	PIA	*C.purpurascens*	RDPCCSNPVCTVHNPQIC*	α6/α3β2β3 (0.95 nM) > α6/α3β4(30.5 nM)>α3β2(74.2 nM)> α3β4(518 nM)	32
	Vc1.1	*C. victoriae*	GCCSDPRCNYDHPEIC*	α9α10 (19 nM) > α6/α3β2β3 (140 nM) > α6/α3β4 (980 nM) > α3β4 (4200 nM) > α3β2 (7300nM)	47
	GIC	*C.geographus*	GCCSHPACAGNNQHIC*	α3β2 (1.1 nM) > α4β2 (309 nM) > α3β4 (755 nM)	32
	TxIB	*C. textile*	GCCSDPPCRNKHPDLC*	α6/α3β2β3 (28.4 nM)	48

[a] αm/n , α-CTxs subgroups (4/6, 4/3, 4/4, 4/7).

[b] *, amidated C-terminal; y, sulfotyrosine; dashes denote gaps; amino acid conservation in the toxin sequences are denoted by shaded segments.

[c] IC_{50}, given IC_{50} values should only act as a rough guide with more detailed information available in the listed references. Most α-CTxs listed were tested on wide range of nAChR subtypes, however only the subtypes for which the peptide is selective and shows less than 10,000nM potency are listed and ranked by potency.

N.D., not determined.

Table 3

$IC_{50}$and Hill slope values for block of various nAChR subtypes by α-CTx TxID.

Subtypes	IC_{50} (nM)[a]	Ratio[b]	Hill slope[a]	Subtypes	IC_{50} (nM)[c]
α3β4	12.5 (9.4–16.5)	1	1.05 (0.66–1.44)	α3β2	>10000[c]
α6/α3β4	94.1 (73–121)	7.5	1.30 (0.73–1.87)	α2β2	>10000[c]
α2β4	4550 (3950–5230)	524	1.95 (1.48–2.42)	α9α10	>10000[c]
α4β4	>10000[c]	--	--	α7	>10000[c]
α4β2	>10000[c]	--	--	Mα1β1δε	>10000[c]
α6/α3β2β3	>10000[c]	--	--		

[a] Numbers in parentheses are 95% confidence intervals;

[b] nAChR subtype IC_{50}/α3β4 IC_{50}

[c] less than 50% block at 10^{-5} M. All receptors are rat except for α1β1δε, which is mouse.

Table 4

Experimental and structural statistics for the 20 lowest energy structures of each TxID isomer

	Isomer 1	Isomer 2
Experimental data		
Distance restraints		
total NOE	102	105
intra-residue	43	38
inter-residue	59	67
sequential (|i-j|)	41	50
medium-range (|i-j|≤4)	18	10
long-range (|i-j|≥5)	0	7
Dihedral angle restraints, φ	6	10
Total NOE violations exceeding 0.3 Å	0	0
Total dihedral violations exceeding 2.0°	0	0
Structure statistics		
Average pairwise rmsd (Å)		
backbone atoms (residues 2–15)	0.48 ± 0.36	0.45 ± 0.25
heavy atoms (residues 2–15)	0.81 ± 0.38	1.13 ± 0.30
Ramachandran statistics[a]		
most favoured and allowed regions, %	95.4	98.3
generously allowed regions, %	4.2	1.7
disallowed regions, %	0.4	0

[a] as analysed by PROCHECK-NMR.